Journal of The Electrochemical Society, **146** (2) 761-766 (1999)
S0013-4651(98)05-078-2 CCC: $7.00 © The Electrochemical Society, Inc.

Two-Dimensional Wafer-Scale Chemical Mechanical Planarization Models Based on Lubrication Theory and Mass Transport

Srikanth Sundararajan,[a,b] Dipto G. Thakurta,[a,b] Donald W. Schwendeman,[c] Shyam P. Murarka,[b,d,*] and William N. Gill[a,b,z]

[a]Department of Chemical Engineering, [b]Center for Integrated Electronics and Electronic Manufacturing, [c]Department of Mathematical Sciences, and [d]Department of Materials Science and Engineering, Rensselaer Polytechnic Institute, Troy, New York 12180, USA

The effects of the variation of chemical mechanical planarization (CMP) process parameters on slurry hydrodynamics and removal rate are studied using physically based models. The two models which are developed to describe and fundamentally understand the CMP process are (*i*) the lubrication model for slurry flow and (*ii*) the mass transport model for material removal. The mass transport model is developed for copper CMP. Conditions for stable operation and reduced wafer scratching are identified from the lubrication model. The mass transport model takes into account the chemical reaction at the wafer surface, the slurry flow hydrodynamics, and the presence of abrasive particles. The polish rates predicted by the model agree well with those measured experimentally.

Manuscript received May 27, 1998.

As the desired feature sizes of semiconductor wafers continue to shrink, the ability to globally planarize the wafer surface becomes increasingly important. Chemical mechanical planarization (CMP) has the capability to achieve adequate local and global planarization necessitated by stringent future submicrometer very large scale integration (VLSI) requirements.[1-3] CMP is now widely accepted for planarizing interlevel dielectrics[4,5] and forming inlaid metal patterns.[6-8]

Figure 1 shows a schematic representation of the CMP process. A rotating wafer is pressed facedown against a rotating polish pad. The wafer and the pad are usually rotated in the same direction and with the same angular velocity, ω, about their respective centers. The polishing slurry containing abrasive particles and chemical reagents is delivered near the center of the polish table. Material is removed from the wafer surface by the combined action of abrasive particles and the chemical reagents. It is known from CMP experiments[9] that the presence of both abrasive particles and chemicals is necessary to produce a desirable polish rate. Hence, it is important to consider this synergistic effect while developing a CMP model. The lower part of Fig. 1 shows a magnified view of the region between the wafer and the polishing pad. The pressure applied to the wafer is supported by the thin slurry film ($h \approx 20$–50 μm) between the wafer and the pad and the thickness of the film, h, is part of the solution of the lubrication model developed in this article.

* Electrochemical Society Fellow.
z E-mail: gillw@rpi.edu

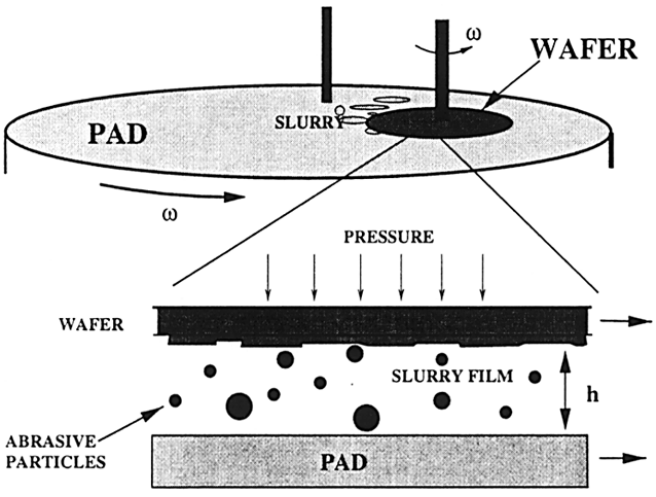

Figure 1. Schematic of CMP process.

The fundamental physical and chemical mechanisms of CMP process are not well understood and, hence, it is desirable to develop physically based models which indicate explicitly the way that these mechanisms depend on the operating and design parameters. Nanz and Camilletti[10] present a good critical review of existing CMP models. Modeling efforts described in the literature range from Preston's equation[11] which is simple to more complex treatment of pad asperities,[12] deformation, and bending.[1,13,14] Although it is known that the slurry forms a thin lubricating film between the wafer and the pad,[15] most of the models do not incorporate the effects of the slurry flow and the chemical reactions which effect CMP. To the authors' knowledge, the first published work which presents a wafer-scale slurry flow analysis is by Runnels and Eyman.[16] They solve the steady-state three-dimensional (3-D) Navier-Stokes equation numerically using a finite-element scheme in the region between the wafer and the pad. Then the process is iterated to obtain a stable position of the wafer which balances the moment about the gimbaling point. Considerable simplifications for solving the slurry flow may be achieved if one recognizes that the reduced Reynolds number is very small and, therefore, the lubrication approximations used in the theory of slider bearings are valid. With these approximations, semianalytical solutions for a 2-D geometry are obtained in this work. Consequently, the analytical approach developed here shows clearly the role of operating conditions and gives a better physical understanding of the influence of process parameters on CMP.

The models described in this article take into account the combined effect of the chemistry and the hydrodynamics of the slurry flow. Two models are developed here which incorporate them together: the lubrication model for slurry flow and the mass transport model. The lubrication model indicates how the parameters interact to determine the velocity, pressure, and thickness in the slurry which give stable operating conditions. The mass transport model uses this velocity field to predict the average polish rate for copper CMP in terms of flow conditions, slurry composition, and particle concentration distributions. The models are evaluated by experiments.

2-D Lubrication Model

Figure 2 shows a schematic of the 2-D lubrication model for slurry flow including the pad and the wafer held by the wafer carrier. The wafer carrier is held by a gimbaling mechanism at the pivot which adjusts itself to a stable position during polishing.[16] The wafer has a certain global curvature as indicated in the figure. The curvature may be represented in terms of the protusion at the center of the wafer. This is referred to as the curvature parameter in this work and is denoted

S0013-4651(98)05-078-2 CCC: $7.00

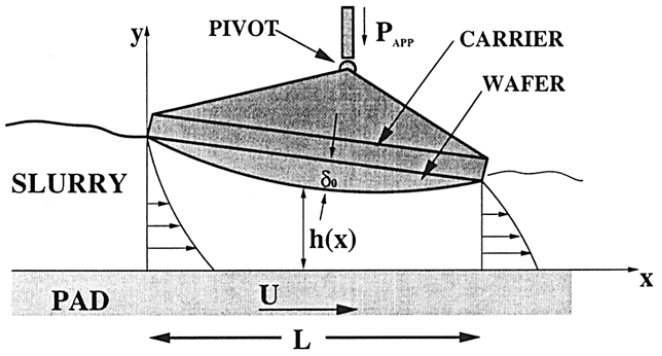

Figure 2. Schematic of 2-D lubrication model for slurry flow.

by δ_0 as shown in the figure. For a 5 in. wafer, δ_0 is in the order of 5 μm. Note that the curvature shown in Fig. 2 is exaggerated for the purpose of illustration. The curvature may arise due to presence of different films on the wafer surface which have different thermal coefficients of expansion. Also, often such a global curvature is imposed by the shape of the wafer-backing film[13] and/or by applying back pressure to help offset excessive material removal at the edges. The wafer and the pad are treated as rigid surfaces in this model.

When both the pad and the wafer rotate in the same direction and with the same angular velocity, ω, it can be shown that any point on the wafer surface has the same relative velocity, $U = \omega R$, with respect to a point on the pad directly below it.[4] The symbol R represents the distance between the centers of the pad and the wafer. Hence, the frame of reference for this 2-D model is the wafer surface. In other words, an observer sitting on the wafer surface would see the pad beneath moving away with a constant velocity U. As the model is 2-D, it does not explicitly incorporate rotation of the wafer relative to the pad. The coordinate axes are shown in Fig. 2 with the origin on the pad surface directly below the left edge of the wafer. The pad motion drags the slurry under the wafer near the left edge and the applied pressure squeezes it out at the right edge of the wafer. The wafer is supported by the pressure, $P(x)$, developed in the slurry film of thickness $h(x)$. The symbol $P(x)$ denotes the pressure in the slurry film above the atmospheric pressure. The problem is to solve for $P(x)$ and $h(x)$ simultaneously. The input parameters for the model are the applied pressure, P_{app}; the diameter of the wafer, L; the pad velocity relative to the wafer, U; the slurry viscosity, μ; and the curvature parameter, δ_0.

Lubrication theory is applied to solve for the pressure, height, and velocity distributions in the slurry film between the pad and the wafer. The slurry is assumed to be a Newtonian incompressible fluid and side flow (flow in the z-direction) is neglected. Lubrication theory is appropriate because the film thickness is small compared to the wafer diameter and the reduced Reynolds number given by

$$Re^* = \frac{\rho U L}{\mu}\left(\frac{\bar{h}}{L}\right)^2 \qquad [1]$$

is small ($\sim 10^{-5}$). In the above equation, $\bar{h}$ is the characteristic thickness of the slurry film which is in the order of micrometers. The pressure developed in the slurry film, $P(x)$, and the slurry film thickness, $h(x)$, are computed according to lubrication theory by solving the Reynolds equation

$$\frac{d}{dx}\left(h^3\frac{dP}{dx}\right) = 6\mu U\frac{dh}{dx} \qquad [2]$$

subject to the boundary conditions

$$P(0) = 0 \qquad P(L) = 0 \qquad [3]$$

Equation 3 implies that the pressure at either edge of the wafer is equal to the atmospheric pressure. For small δ_0, the shape of the convex wafer surface can be taken as a parabola to a good approximation. Hence, the surface of the wafer is described by

$$h(x) = h_1 + \{h_0 - h_1\}\left(1 - \frac{x}{L}\right) - 4\delta_0\left(\frac{x}{L}\right)\left(1 - \frac{x}{L}\right) \qquad [4]$$

where h_0 and h_1 are the height of the film at the left and the right edge of the wafer, respectively. These parameters are determined later to balance the load and moment on the wafer. Two more constraints are needed to solve Eq. 2 as $h(x)$ depends on the unknown heights h_0 and h_1. These constraints are

$$\frac{1}{L}\int_0^L P(x)dx = P_{app} \qquad [5]$$

which implies that the average pressure developed in the slurry film must balance the load on the wafer, and

$$\frac{\int_0^L P(x)\,x\,dx}{\int_0^L P(x)dx} = \frac{L}{2} \qquad [6]$$

which implies that the moment of force about the center of the wafer is zero. Equation 2 and the boundary conditions in Eq. 3 can be solved analytically for $P(x)$ and then the two integral constraints for h_0 and h_1 can be satisfied using numerical quadrature. The solution set $\{P(x), h_0, h_1\}$ is a function of the known parameters $\{P_{app}, L, U, \mu, \delta_0\}$.

The hydrodynamic lubrication model indicates that a positive fluid pressure is developed in the gap between the wafer and the pad and this supports the applied load. Experimental film thickness measurements by Nakamura et al.[15] confirm this hydrodynamic regime of CMP operation. To the contrary, Levert[17] measured experimentally a suction or negative fluid pressure beneath the wafer. This implies that the applied load is supported by solid-solid contact between the wafer and the pad asperities. It is noted that higher applied pressures (~30 kPa) and lower relative pad velocities (~0.7 m/s) are used in Ref. 17, and these conditions are less favorable for hydrodynamic lubrication. Also, the shape of the wafer and the pad properties are important in determining the regime of operation.

After the pressure distribution, $P(x)$, together with the heights, h_0 and h_1, are known, the velocity distributions can be computed. According to lubrication theory, the x-component of the velocity is given by

$$u(x, y) = U\left(1 - \frac{y}{h(x)}\right) - \frac{dP}{dx}\frac{h^2(x)}{2\mu}\frac{y}{h(x)}\left(1 - \frac{y}{h(x)}\right) \qquad [7]$$

and the y-component $v(x, y)$ follows from the equation of continuity. These velocity components satisfy the no-slip boundary condition and a condition of the zero normal flow at the pad and wafer surfaces.

The solutions for three representative cases with different values for P_{app} and U are presented in Fig. 3, 4, and 5. These three solutions are obtained using $L = 5$ in. and $\delta_0 = 5$ μm. The slurry viscosity is taken to be the same as that for water ($\mu = 0.001$ Pa s) assuming the slurry mixture is sufficiently dilute. Figure 3 shows the solution for $P_{app} = 14$ kPa and $U = 1.3$ m/s. The x-axis gives the axial position. The wafer surface, $h(x)$, is shown on the left ordinate, and the pressure, $P(x)$, developed in the slurry film is shown on the right ordinate. The heights h_0 and h_1 are equal to 59 and 40 μm, respectively, as shown in the figure. The shape of the pressure distribution in the slurry is approximately parabolic. This pressure distribution supports the applied pressure of 14 kPa. A maximum pressure of 21 kPa is developed near the center of the wafer. The slurry velocity profiles, normalized with respect to U, are shown at $x = 0$ and L, and these profiles have different shapes due to the pressure distribution in the slurry film. The slurry is dragged in the positive x-direction by the no-slip boundary condition at the pad while it experiences an adverse pressure gradient at $x = 0$ and a favorable one at $x = L$. This causes the velocity profile to be fuller at the exit as seen in Fig. 3.

S0013-4651(98)05-078-2 CCC: $7.00

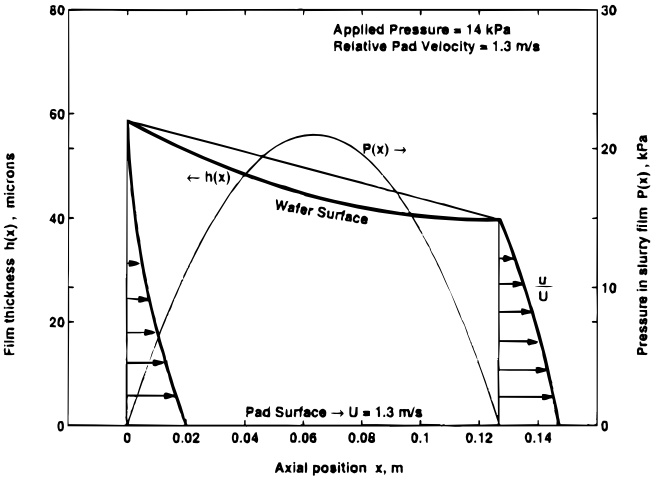

Figure 3. Case (a): Pressure distribution and velocity profiles for P_{app} = 14 kPa, U = 1.3 m/s, L = 5 in, μ = 0.001 Pa s, and δ_0 = 5 μm.

Figures 4 and 5 show the effect of an increased applied pressure and a decreased pad velocity, respectively. For the case of an increased applied pressure, there is a greater adverse pressure gradient at the inlet. For the case of a decreased pad velocity, the slurry has a lower kinetic energy entering the gap. Both of the these effects result in a thinner velocity profile at the inlet, $x = 0$, and for the chosen parameter values a region of reverse flow exists as indicated in the figures. Also, note that the height of the gap between the pad and the wafer is decreased in both cases.

Reverse flow causes slurry recirculation and may lead to flow instabilities. This in turn will result in nonuniform polish rates at the edges. Hence, it is important to identify when reverse flow occurs based on the known parameters of the CMP process. A condition for reverse flow is

$$\frac{\partial u(0,\ h_0)}{\partial y} > 0 \qquad [8]$$

given the wafer-pad geometry in Fig. 1, which, using Eq. 7, leads to a condition that takes the form

$$\frac{dP(0)}{dx} > \frac{2\,\mu U}{h_0^2} \qquad [9]$$

Using the solutions for the pressure, $P(x)$, and h_o and Eq. 9, the condition for reverse flow becomes

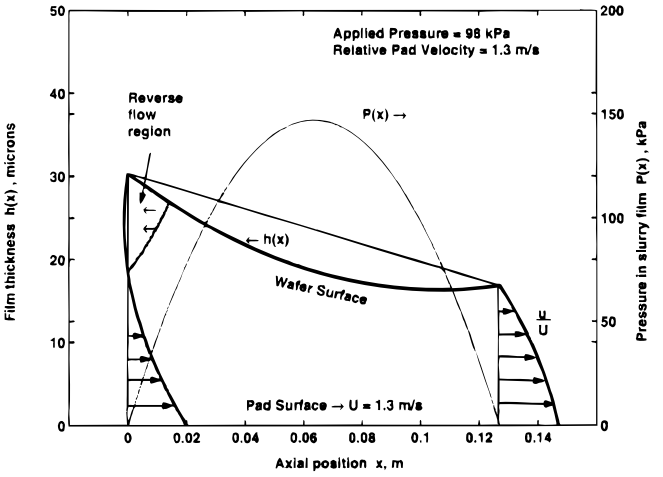

Figure 4. Case (b): The effect of increased applied pressure on stability of slurry flow (P_{app} = 98 kPa, U = 1.3 m/s, L = 5 in, μ = 0.001 Pa s, and δ_0 = 5 μm).

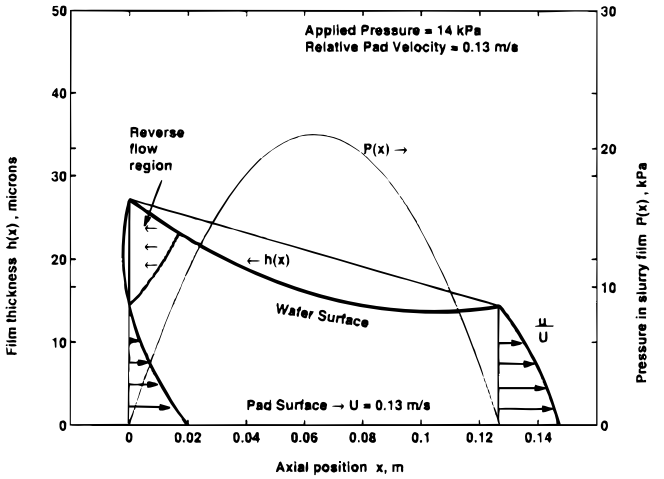

Figure 5. Case (c): Effect of reduced relative pad velocity on stability of slurry flow (P_{app} = 14 kPa, U = 0.13 m/s, L = 5 in, μ = 0.001 Pa s, and δ_0 = 5 μm).

$$\delta_0 < 0.085\sqrt{\frac{\mu UL}{P_{app}}} \qquad [10]$$

Other important quantities which may be obtained from the model are the average fluid shear stress at the wafer surface, τ_w, and the minimum separation between the pad and the wafer, h_{min}. The first quantity, τ_w, is important in determining the polish rate. Runnels[18] feature-scale fluid-based erosion model is based on the assumption that the polish rate is proportional to the shear stress at the wafer surface. The average shear stress on the wafer surface due to the slurry, τ_w, is given by

$$\tau_w = \frac{1}{L}\int_0^L \mu\left|\frac{\partial u(x,\ h(x))}{\partial y}\right| dx \qquad [11]$$

The latter quantity, h_{min}, is believed to be important in scratching. The wafer surface can be scratched by direct rubbing of the pad against the wafer during CMP. Hence, it is hypothesized that a larger separation between the wafer and the pad, i.e., a larger h_{min}, is better for preventing scratches. Figure 6 shows the behavior of dimensionless forms of τ_w and h_{min} as a function of a dimensionless curvature parameter, $\delta_0/\sqrt{\mu UL/P_{app}}$. These curves become approximately constant as the dimensionless curvature parameter increases to the value of 0.085 indicated in Eq. 10. Thus, the shear stress at the wafer surface and, hence, the polish rate increases as either U or P_{app} is increased. Similarly, the thickness of the slurry film increases as U is increased or

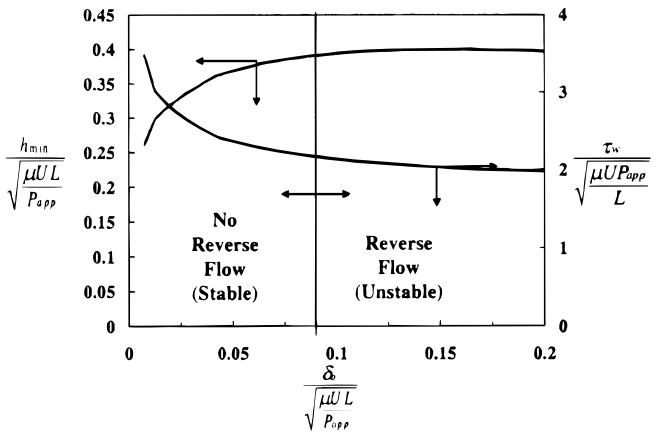

Figure 6. Generalized dimensionless plot showing how operating conditions and curvature affect CMP performance parameters.

S0013-4651(98)05-078-2 CCC: $7.00

if P_{app} is decreased while holding the other parameters fixed. These results are consistent with those presented by Runnels and Eyman.[16] Also, it is seen that increasing the viscosity of the slurry increases both τ_w and h_{min}, which leads to higher polish rates and less scratching.

The present model gives a clear picture of the slurry flow profiles at the inlet and outlet and a criterion for reverse flow is identified. In the next section, a mass transport model is developed, which employs the velocity field between the wafer and pad. The mass transport model predicts the polish rate, which can be compared readily with CMP experiments.

Mass Transport Model for Copper CMP

The slurry flow velocities computed using the lubrication model are independent of the type of CMP process chemistry. But, the mass transport depends on the type of material to be polished, the slurry chemistry, and the abrasive particles. So, a process-specific mass transfer model is necessary. In this article, the mass transport model is developed based on the chemistry of copper CMP.

Preliminary copper CMP experiments were performed. Five-inch wafers with sputtered blanket copper film are used for the polishing experiments. The slurry has three components: (*i*) an oxidizing agent, potassium ferricyanide [$K_3Fe(CN)_6$], 0–6 wt %, (*ii*) a complexing agent, ammonium hydroxide (NH_4OH), 0–3 vol %, and (*iii*) abrasive, alumina particles (0.06 μm nominal diam). Deionized (DI) water is added to the above to make up the slurry. This slurry chemistry was developed by Steigerwald.[9] The mechanism of copper removal during CMP is a three step process[19]: (*i*) formation of a passivating surface layer, (*ii*) mechanical abrasion of the surface layer, and (*iii*) chemical dissolution of the resulting abraded material. In short, copper CMP occurs by abrasive assisted chemical dissolution of the surface.

An IPEC 372M Westech polishing tool is used with a SUBA 500 pad manufactured by Rodel. The diameter of the polishing table is approximately 22.5 in. and the eccentric distance between the polishing head and the center of the polishing table, *R*, is 5.6 in. For example, the wafer and the pad both rotating in the same direction at 90 rpm in this configuration gives a relative pad velocity of U = 1.3 m/s. The slurry delivery rate is approximately 80–100 mL/min. The polish time varies from 1 to 2 min. Average sheet resistance is measured using a four-point probe before and after the polishing experiment to calculate the average thickness of the copper film, which in turn is used to compute an average polish rate. Further experimental details may be found in the thesis by Sundararajan.[20]

Electrochemical measurements by Sainio et al.[21] suggest that copper in ammonia-based slurries dissolves to form a cuprous diammine complex $Cu(NH_3)_2^+$. The dissolution reaction of copper for the used slurry chemistry is

$$Cu + Fe(CN)_6^{3-} + 2NH_3 \overset{K_{eq}}{\rightleftharpoons} Cu(NH_3)_2^+ + Fe(CN)_6^{4-} \quad [12]$$

where K_{eq} is the equilibrium constant for the reaction. It is assumed that reaction 12 is fast and proceeds quickly to equilibrium at the wafer surface. Then, the equilibrium concentration of the dissolved copper species, $Cu(NH_3)_2^+$, at the wafer surface, C_s, is given by

$$C_s = \sqrt{K_{eq}}\sqrt{C_F}C_N \quad [13]$$

for small concentrations of C_s. In Eq. 13, C_F is the potassium ferricyanide concentration and C_N is the ammonium hydroxide concentration in the slurry. Both, C_F and C_N are assumed to be uniform in the slurry. These concentrations may be computed from the composition of the slurry.

The dissolved copper species diffuses from the wafer surface and is carried away by the slurry. The following mass transport equation can be written for the concentration, $C(x, y)$, of the dissolved species

$$u\frac{\partial C}{\partial x} + v\frac{\partial C}{\partial y} = D\frac{\partial^2 C}{\partial y^2} \quad [14]$$

In the above equation, D is the diffusivity of the dissolved copper species. The value of D used for this work is 10^{-9} m^2/s based on mass transfer studies by Zembura et al.[22] The contribution to the diffusion in the x-direction is neglected because $h << L$. The slurry velocities u and v are taken from the lubrication model, and the boundary conditions for Eq. 14 are

$$C(x, h(x)) = C_s \quad [15]$$

$$\frac{\partial C(x, 0)}{\partial y} = 0 \quad [16]$$

and

$$C(0, y) = 0 \quad [17]$$

Equation 15 implies that the concentration of the dissolved copper species at the wafer surface is given by its equilibrium concentration as described in Eq. 13. Equation 16 implies an impenetrable pad surface and Eq. 17 assumes that the fresh slurry coming in at $x = 0$ has no dissolved copper in it. Equation 14 is solved numerically[20] using the NAG library subroutine D03CF[23] along with the boundary conditions in Eq. 15-17, where C_s is given by Eq. 13. The total flux of copper, J_s, leaving the wafer surface is given by

$$J_s = \frac{1}{L}\int_0^L D\frac{\partial C(x, h)}{\partial y}dx \quad [18]$$

Since the polish rate depends directly on the amount of copper lost from the wafer surface, Eq. 18 is a measure of the polish rate.

With certain simplifications, an analytical solution of Eq. 14 can be obtained which gives results close to the numerical solution and provides a more general understanding of the problem of how the process parameters affect CMP. The simplifying assumptions are discussed below.

1. Since the computed pressure profiles resemble the shape of a parabola, a parabolic pressure distribution is assumed in the slurry film. The approximate pressure profile satisfies Eq. 3, 5, and the moment balance condition, Eq. 6. It is given by

$$P(x) \simeq 6P_{app}\left\{\frac{x}{L} - \left(\frac{x}{L}\right)^2\right\} \quad [19]$$

2. For purposes of obtaining an analytical solution for the mass transport calculations, the separation between the pad and the wafer, $h(x)$, is assumed to be constant with a value $h \simeq h_{min}$. This is justified as the mass transport is important only in the concentration boundary layer which develops near the surface of the wafer.

Using the approximate parabolic pressure profile, an analytical expression for $u(x, y)$ is obtained using Eq. 7 which is then expanded in a first order Taylor series for the region close to the wafer where the concentration gradients are large. The expression for v follows from the equation of continuity. The expressions of u and v thus obtained are given by

$$u \simeq U\left[1 - \phi\left(1 - \frac{2x}{L}\right)\right]\frac{h_{min} - y}{h_{min}} \quad [20]$$

$$v \simeq U\phi\frac{(h_{min} - y)^2}{h_{min}L} \quad [21]$$

where ϕ is a dimensionless quantity given by $\phi = (3\,h_{min}^2 P_{app})/\mu UL$). Using an approximate value of h_{min} from Fig. 6, one obtains $\phi \simeq 0.37$. An analytical solution for C, valid in a boundary layer near $h = h_{min}$, can be obtained from Eq. 14 with the approximations for u and v given by Eq. 20 and 21, respectively. Using the scaled variables $\eta = (h_{min} - y)/(h_{min}\Delta(\xi))$ and $\xi = x/L$, where the dimensionless boundary layer thickness $\Delta(\xi)$ is determined by solving

$$\frac{d\Delta^3}{d\xi} + \frac{3\phi\Delta^3}{(1 - \phi) + 2\phi\xi} = \frac{\left(\frac{9D}{h_{min}U}\right)\left(\frac{L}{h_{min}}\right)}{1 - \phi + 2\phi\xi} \quad [22]$$

S0013-4651(98)05-078-2 CCC: $7.00

with the boundary condition $\Delta(0) = 0$, the equation for C becomes

$$\frac{d^2C}{d\eta^2} + 3\eta^2 \frac{dC}{d\eta} = 0 \qquad [23]$$

The solution for C follows by solving Eq. 23 subject to the boundary conditions $C(\eta = 0) = C_s$ and $C(\eta = \infty) = 0$. From the solution, the flux of copper away from the wafer surface is given by

$$D\frac{\partial C(x, h_{\min})}{\partial y} = -\frac{D}{h_{\min}\Delta}\frac{dC(0)}{d\eta} = \frac{D}{h_{\min}\Delta}\frac{C_s}{\Gamma(4/3)} \qquad [24]$$

where Γ is the gamma function, $\Gamma(4/3) = 0.893$, and Δ is the solution of Eq. 22 given by

$$\Delta(\xi) = \left\{\frac{3}{\phi}\frac{D}{h_{\min}U}\frac{L}{h_{\min}}\left[1 - \left(1 + \frac{2\phi\xi}{1-\phi}\right)^{-\frac{3}{2}}\right]\right\}^{-3} \qquad [25]$$

Equation 24 is used with Eq. 18 to obtain the average copper flux leaving the wafer surface

$$J_s = \frac{DC_s}{0.893}\left\{\frac{1}{h_{\min}}\int_0^L \frac{d\xi}{\Delta(\xi)}\right\} = \frac{DC_s}{0.893}\frac{1}{\Delta_{avg}} \qquad [26]$$

In Eq. 26, $1/\Delta_{avg}$ is used to denote the quantity in the curly braces for convenience.

The abrasive particles undergo rotational and linear motion in the shear flow. This motion of the abrasive particles enhances the dissolution rate of the surface by facilitating the liquid phase convective mass transfer of the dissolved copper species away from the wafer surface. It is proposed that the enhancement in polish rate is directly proportional to the product of abrasive concentration and the shear stress at the wafer surface. Hence, the ratio of polish rate with abrasive to the polish rate without abrasive can be written as

$$\frac{\text{Polish rate with abrasives}}{\text{Polish rate without abrasives}} = 1 + \alpha\tau_w C_A \qquad [27]$$

where α is the proportionality constant and C_A is the abrasive concentration (wt %) in the slurry. The proportionality constant is the abrasive enhancement factor α which is determined from polish experiments with and without abrasive particles. Figure 7 shows that the experiments corroborate Eq. 27 and they indicate that α is approximately 0.665.

Taking into account the enhancement caused by the abrasives, the expression for average polish rate, R_p becomes

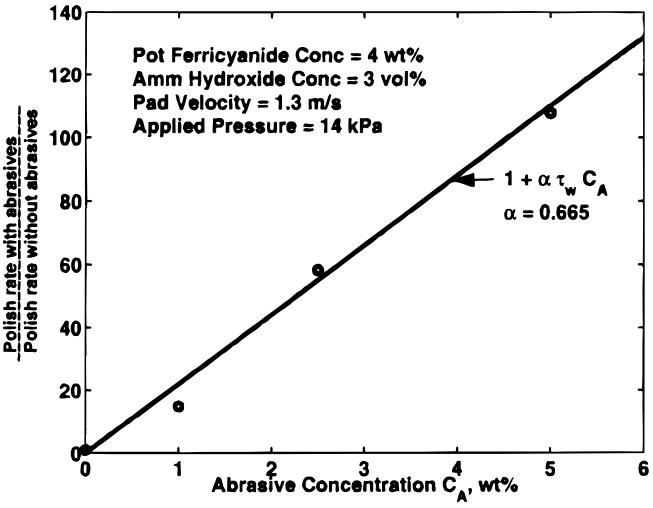

Figure 7. Determination of abrasive enhancement factor, α.

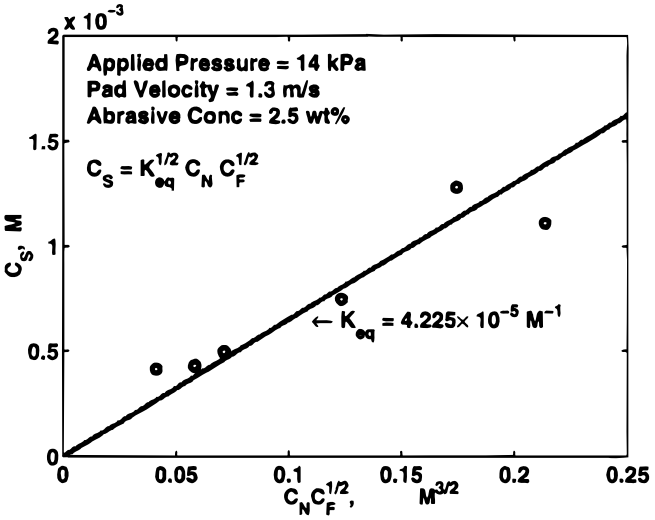

Figure 8. Determination of equilibrium constant, K_{eq}.

$$R_p = \frac{M_{Cu}}{\rho_{Cu}} \times J_s \times (1 + \alpha\tau_w C_A)$$

$$= \frac{M_{Cu}}{\rho_{Cu}} \times \frac{D\sqrt{K_{eq}C_F}C_N}{0.893\ \Delta_{avg}} \times (1 + \alpha\tau_w C_A) \qquad [28]$$

where M_{Cu} and ρ_{Cu} are the molecular weight and density of copper, respectively. The value of K_{eq} is determined from the experimental data plotted in Fig. 8. These data agree well with the assumption that the interfacial reaction proceeds quickly to equilibrium as indicated in Eq. 13, and they yield the value of $K_{eq} = 4.225 \times 10^{-5}$ mol^{-1}.

The model given by Eq. 28 is evaluated with the preliminary experimental data given in Fig. 9 and 10. Figure 9 shows the experimental data and model predictions for $P_{app} = 14$ kPa and $U = 1.3$ m/s for different potassium ferricyanide wt % and two different ammonium hydroxide vol %. The polish rate increases with both potassium ferricyanide wt % and ammonium hydroxide vol %. Figure 10 shows the experimental data and model predictions for a reduced relative pad velocity $U = 0.65$ m/s. The polish rates decrease when U is decreased, and there is reasonable agreement between the model and the experiments. Other parameters used in

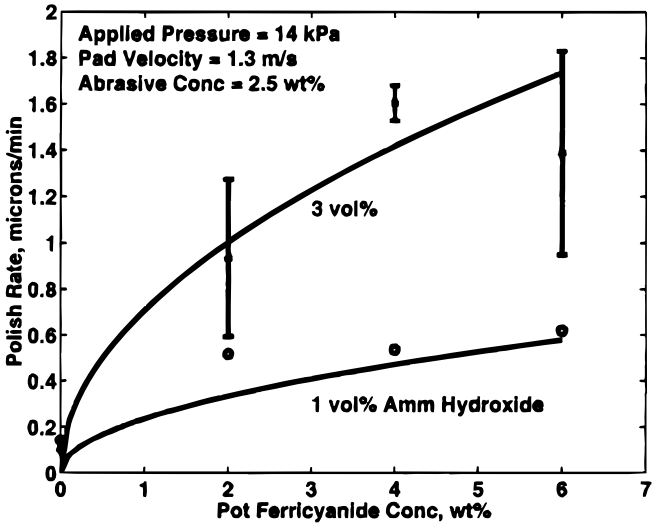

Figure 9. Comparison of model with experiment, $U = 1.3$ m/s and $P_{app} = 14$ kPa.

S0013-4651(98)05-078-2 CCC: $7.00

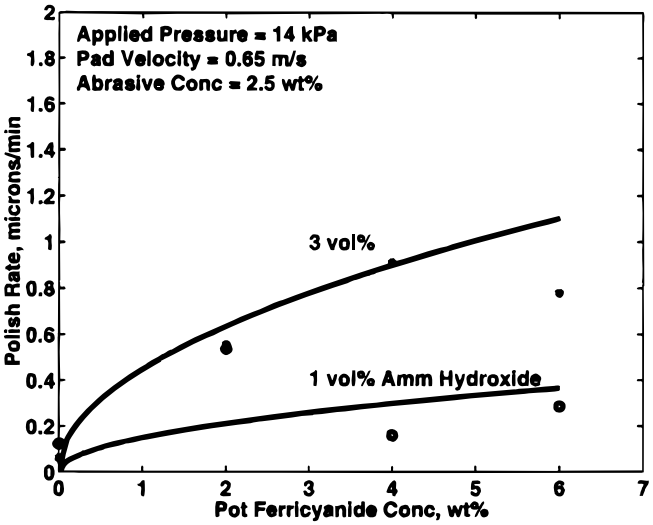

Figure 10. Comparison of model with experiment, $U = 0.65$ m/s and $P_{app} = 14$ kPa.

the model predictions are $L = 5$ in., $\mu = 0.001$ Pa s, $\delta_0 = 5$ μm, and $C_A = 2.5$ wt % for both figures.

Conclusions

Two models are developed: (*i*) lubrication model for slurry flow and (*ii*) mass transport model. The development of the lubrication model is based on hydrodynamics of slider-bearing theory. It includes developing and solving the Reynolds equation to compute simultaneously (*i*) the pressure distribution developed in the thin slurry film between the pad and wafer and (*ii*) the thickness of the slurry film which is the distance between the pad and wafer for different operating conditions. The model shows that the applied pressure on the wafer is supported by the pressure developed in the thin slurry film present between the wafer and the polishing pad. The thickness of the slurry is about 20–50 μm between the pad and the wafer and depends on operating conditions. The film thickness and the shear stress on the wafer surface are scratching parameters. It appears that thicker and more viscous films together with lower shear lead to smoother films with less scratching. Scratch-free CMP is a good indication of a robust CMP process and the motivation is to be able to understand the process well for materials that will be used in the next decade. The shear can be reduced and the thickness increased by lowering the applied pressure on the pad. But, decreasing the shear leads to reduced polish rate. Hence, a balance between reducing scratching and achieving an acceptable polish rate is necessary. The lubrication model also predicts the conditions for which reverse flow may occur at the edges of the wafer and these should be avoided in practice. The reverse flow can cause flow instabilities and nonuniformities in the polished surface. Criteria for stable operations are identified from the model.

The mass transfer model is developed using the results of the slurry flow model to predict the polish rates of copper CMP as a function of operating conditions and slurry composition. The dissolved copper species is convectively diffused and forms a concentration boundary layer in the slurry between the wafer and the pad. The flow field (of slurry thin film) that is obtained from the lubrication model is used in the mass transfer model. An analytical solution of the mass transfer model is obtained which agrees very well with the numerical results. It is important that the mass transport model takes into account the slurry chemistry, the effect of the abrasive, and the hydrodynamics of the flow. The model predictions of the polish rate with are in good agreement preliminary experiments.

Acknowledgment

This work was supported by the New York Sematech Center of Excellence, SRC contract number 97-IC-448.

Rensselaer Polytechnic Institute assisted in meeting the publication costs of this article.

References

1. S. Sivaram, H. Bath, R. Leggett, A. Maury, K. Monnig, and R. Tolles, *Solid State Technol*., **35**, 87 (1992).
2. I. Ali, S. R. Roy, and G. Shinn, *Solid State Technol*., **37**, 63 (1994).
3. J. M. Steigerwald, S. P. Murarka, and R. J. Gutmann, *Chemical Mechanical Planarization of Microelectronic Materials*, Wiley-Interscience, New York (1997).
4. W. J. Patrick, W. L. Guthrie, C. L. Standley, and P. M. Schiable, *J. Electrochem. Soc*., **138**. 1778 (1991).
5. P. A. Burke, in *Proceedings of the 8th International IEEE VLSI Multilevel Interconnection Conference (VMIC)*, p. 379, Santa Clara, CA, June 11-12 (1991).
6. F. B. Kaufman, D. B. Thompson, R. E. Broadie, M. A. Jaso, W. L. Guthrie, D. J. Pearson, and M. B. Small, *J. Electrochem. Soc*., **138**, 3460 (1991).
7. H. Landis, P. Burke, W. Cote, W. Hill, C. Hoffman, C. Kaanta, C. Koburger, W. Lange, M. Leach, and S. Luce, *This Solid Films*, **220**, 1 (1992).
8. J. M. Steigerwald, R. Zirpoli, S. P. Murarka, D. Price, and R. J. Gutmann, *J. Electrochem.Soc*., **141**, 2842 (1994).
9. J. M. Steigerwald, Ph.D. Thesis, Rensselaer Polytechnic Institute, Troy, NY (1995).
10. G. Nanz and L. E. Camilletti, *IEEE Trans. Semicond. Manuf.*, **8**, 382 (1995).
11. F. Preston, *J. Soc. Glass Technol*., **11**, 247 (1927).
12. T.-K. Yu, C. C. Yu, and M. Orlowski, *Tech. Dig. Int. Electron Devices Meet.*, 865 (1993).
13. S. R. Runnels and P. Renteln, *Dielectric Sci. Technol*., 110 (1993).
14. D. Wang, J. Lee, K. Holland, T. Bibby, and T. Cale, *J. Electrochem. Soc*., **141**, 2843 (1997).
15. T. Nakamura, K. Akamatsu, and N. Arakawa, *Bull. Jpn. Soc. Precis. Eng.*, **19**, 120 (1985).
16. S. R. Runnels and L. M. Eyman, *J. Electrochem. Soc*., **141**, 1698 (1994).
17. J. A. Levert, Ph.D. Thesis, Georgia Institute of Technology, Atlanta, GA (1997).
18. S. R. Runnels, *J. Electrochem. Soc*., **141**, 1900 (1994).
19. J. M. Steigerwald, S. P. Murarka, J. Ho, R. J. Gutmann, and D. J. Duquette, *J. Vac. Sci. Technol., B*, **13**, 2215 (1995).
20. S. Sundararajan, M.S. Thesis, Rensselaer Polytechnic Institute, Troy, NY (1997).
21. C. A. Sainio, D. J. Duquette, J. M. Steigerwald, and S. P. Murarka, *J. Electron. Mater*., **25**, 1593 (1996).
22. Z. Zembura, A. Piotrowski, and Z. Kolenda, *J. Appl. Electrochem*., **20**, 365 (1990).
23. NAG Fortran Library, Numerical Algorithms Group Inc., Downers, Grove, IL (1996).